Inorg. Chem. **2007**, *46*, 8051–8058

Transition-Metal-Induced Fluorescence Resonance Energy Transfer in a Cryptand Derivatized with Two Different Fluorophores

Kalyan K. Sadhu, Bamaprasad Bag, and Parimal K. Bharadwaj*

Chemistry Department, Indian Institute of Technology Kanpur, Kanpur 208016 India

Received March 15, 2007

A laterally nonsymmetric aza cryptand has been derivatized with one 7-nitrobenz-2-oxa-1,3-diazole (fluorophore$_1$) and one/two anthracenes (fluorophore$_2$) to obtain **1** and **2**. Their emission characteristics are probed in the presence of a number of transition metals and proton. In the case of **1**, Cu(II), Zn(II), Cd(II), and proton afford a large enhancement of fluorescence, whereas Fe(II) and Ag(I) exhibit one order of magnitude less enhancement. In contrast, **2** gives a large enhancement with Cu(II), Ag(I), and proton. The enhancement is observed in the diazole moiety even when the anthracene fluorophore is excited because of substantial fluorescence resonance energy transfer from anthracene to the diazole moiety. Compounds **1** and **2** can be termed as the second-generation fluorescence signaling systems.

Introduction

Fluoroionophores have been built[1−5] that report the binding of a guest to the host with an increase or decrease in fluorescence quantum yields. Two design principles[3,6] are mainly adopted for this: (i) both the signaling (fluorophore(s)) and the guest binding (receptor) moieties are integrated into a single unit, or (ii) fluorophore(s) and the receptor are connected through a spacer that acts as a conduit for electronic communication between the two. Because the later design is modular in nature, both the fluorophore and the receptor can be varied easily. Here, the receptor can be modified to induce selectivity in the binding of a guest and to allow for probing of new strategies of fluorescence detection. We have used a cryptand as a receptor, where a metal ion forms a highly stable inclusion complex due to the cryptate effect.[6a] In the absence of a metal ion, the fluorophore, when excited, does not show any emission as a result of intramolecular photoinduced electron transfer (PET)[7] from the lone pair of electrons on the nitrogen atom to the fluorophore, and the excited fluorophore comes down to the ground state through a nonradiative pathway. In the presence of a suitable metal ion as an input to the system, the PET is blocked because of the engagement of the nitrogen lone pair of electrons to the metal and fluorescence can be observed. Because transition metals quench fluorescence effectively, different design strategies have been pursued[8] to surmount this problem. We had shown earlier that efficient fluorescence signaling by transition-metal ions could be built with cryptands as receptors.[9]

In systems containing more than one type of fluorophore in which the emission spectrum of one overlaps with the absorption spectrum of the other, substantial fluorescence resonance energy transfer[10] can take place. This design

* To whom correspondence should be addressed. E-mail: pkb@iitk.ac.in.

(1) (a) Lehn, J.-M. *Supramolecular Chemistry − Concepts and perspectives*; VCH Publishers: Weinheim, Germany, 1995. (b) Valeur, B. In *Topics in Fluorescence Spectroscopy*; Lakowicz, J. R., Ed.; Plenum Press: New York, 1994; Vol. IV. (c) Czarnik, A. W. *Acc. Chem. Res*. **1994**, *27*, 302.

(2) (a) Valeur, B.; Leray, I. *Coord. Chem. Rev*. **2000**, *205*, 3. (b) de Silva, A. P.; Tecilla, P. *J. Mater. Chem*. **2005**, 15.

(3) Callan, J. F.; de Silva, A. P.; Magri, D. C. *Tetrahedron* **2005**, *61*, 8551.

(4) Rurack, K. *Spectrochim. Acta, Part A* **2001**, *57*, 2161.

(5) Fabbrizzi, L.; Poggi, A. *Chem. Soc. Rev.* **1995**, *25*, 197.

(6) (a) Bharadwaj, P. K. *Prog. Inorg. Chem.* **2003**, *51*, 251. (b) Canary, J. W.; Gibb, B. C. *Prog. Inorg. Chem*. **1997**, *45*, 1. (c) Bissell, R. A.; de Silva, A. P.; Gunaratne, H. Q. N.; Lynch, P. L. M.; Maguire, G. E. M.; McCoy, C. P.; Sundanayake, K. R. A. S. *Top. Curr. Chem*. **1993**, *168*, 223. (d) Bissell, R. A.; de Silva, A. P.; Gunaratne, H. Q. N.; Lynch, P. L. M.; Maguire, G. E. M.; McCoy, C. P.; Sundanayake, K. R. A. S. *Chem. Soc. Rev.* **1992**, 137.

(7) Kavarnos, G. J. *Fundamentals of Photoinduced Electron Transfer*; VCH Publishers: Weinheim, Germany, 1993.

(8) (a) Rurack, K.; Resch-Genger, U. *Chem. Soc. Rev.* **2002**, *31*, 116. (b) de Silva, A. P.; Gunaratne, H. Q. N.; Gunnlaugsson, T.; Huxley, A. J. M.; McCoy, C. P.; Rademacher, J. T.; Rice, T. E. *Chem. Rev*. **1997**, *97*, 1515.

(9) (a) Ghosh, P.; Bharadwaj, P. K.; Roy, J.; Ghosh, S. *J. Am. Chem. Soc*. **1997**, *119*, 11903. (b) Bag, B.; Bharadwaj, P. K. *Inorg. Chem*. **2004**, *43*, 4626. (c) Bag, B.; Bharadwaj, P. K. *Org. Lett*. **2005**, *7*, 1573.

(10) (a) Förster, T. *Z. Naturforsch.* **1949**, *49*, 321. (b) Cheung, H. C. In *Topics in Fluorescence Spectroscopy*; Lakowicz, J. R., Ed.; Plenum Publishing: New York, 1991; Vol. 2, p 128.

10.1021/ic700506r CCC: $37.00
Published on Web 08/15/2007

strategy allows for ratiometric[11] fluorescence signaling and offers a new generation of fluorescence sensors. Because the fluorescence resonance energy transfer also depends on the distance and orientation of the two fluorophores, it becomes an important biological tool to monitor[12] enzyme activity and conformational analysis[13] of protein structures. Besides, this is potentially important[14] in pharmacology, dye lasers, frequency conversion of light, and so on. A cryptand is attractive for studying fluorescence resonance energy transfer because it can act as a perfect skeleton to sequentially add different fluorophores. Besides, it can undergo conformational changes[9c] to enable partial movement of one of the side arms with respect to another, which changes the distance and the orientation of the fluorophores with respect to one another, with implications on the fluorescence resonance energy transfer efficiency. Herein, we report the synthesis of an aza−oxa cryptand derivatized with one 7-nitrobenz-2-oxa-1,3-diazole (hereafter, diazole) and one/two anthracene groups through methylene spacers. The emission band of anthracene overlaps with the absorption band of diazole, making it a fluorescence resonance energy transfer system. When the cavity is empty, no significant interaction between the fluorophores takes place. However, when a metal ion or proton is added, the PET is blocked, and the fluorescence resonance energy transfer is switched on. Both solid-state and solution fluorescence measurements are reported along with absorption data.

Scheme 1. Synthetic Route to the Investigated Compounds **1** and **2**[a]

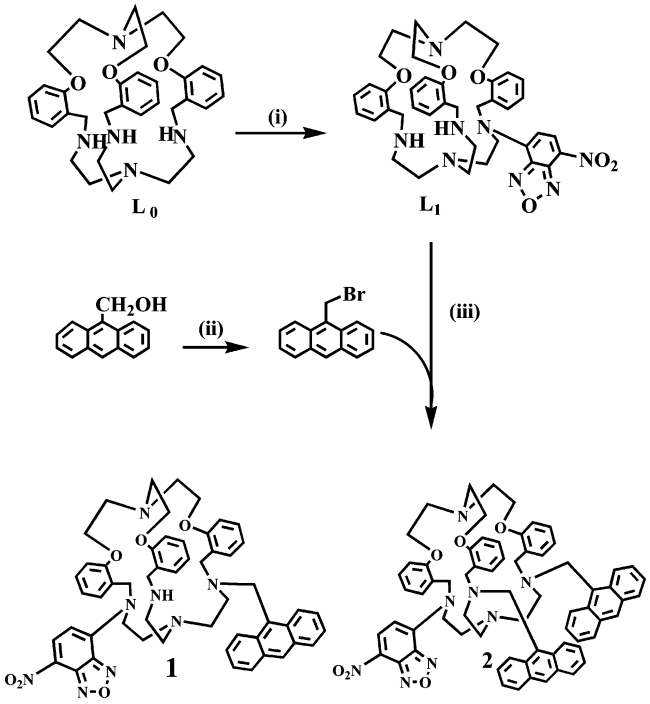

[a] Reagent and conditions: (i) 4-chloro-7-nitrobenz-2-oxa-1,3-diazole, toluene, refluxed for 6 h; (ii) PPh_3, Br_2, MeCN, 25 °C; (iii) K_2CO_3, MeCN, KI, refluxed for 48 h.

Experimental Section

Materials. All of the solvents and thionyl chloride were purified prior to use. The purified solvents were found to be free from impurities and moisture and were transparent in the region of interest. All of the other reagent-grade chemicals including metal salts were acquired from Aldrich and were used as received. The metal salts were hydrated as mentioned in the Aldrich catalog. For chromatographic separation, 100−200 mesh silica gels (Acme Synthetic Chemicals) were used. The reactions were carried out under a N_2 atmosphere, unless otherwise mentioned.

Synthesis. The synthetic route for the cryptand derivatives is illustrated in Scheme 1. Cryptand $\mathbf{L_0}$ was synthesized and recrystallized from acetonitrile as colorless rectangular crystals following our previously reported[15] procedure.

Synthesis of $\mathbf{L_1}$. Compound $\mathbf{L_1}$ was synthesized following the procedure reported previously[9b] from our laboratory.

Synthesis of 1 and 2. To a solution of $\mathbf{L_1}$ (0.36 g, 0.5 mmol) in dry acetonitrile (20 mL) was added anhydrous K_2CO_3 (1.5 g, excess), and the solution was stirred for 15 min. Freshly recrystallized 9-bromomethyl anthracene[16] (0.21 g, 0.75 mmol) was added to it along with a crystal of KI, and the reaction mixture was allowed to reflux for 72 h. After cooling to room temperature, K_2CO_3 was removed by filtration. The yellow filtrate was evaporated to dryness under reduced pressure, washed several times with water, and then extracted with $CHCl_3$. The organic layer, after drying over anhydrous Na_2SO_4, evaporated to dryness to obtain a yellow solid that was a mixture of **1** and **2**.

Compound 2. This product was eluted out with a mixture of chloroform and methanol (98:2 (v/v)) as the eluent. The dark-red solid obtained upon evaporation of the solvent was recrystallized from acetone. Yield: 30%. Mp: 256 °C. ^{1}H NMR (400 MHz, $CDCl_3$, 25 °C, TMS, δ): 0.81 (t, 4H, 2 × CH_2), 1.10 (s, 4H, 2 × CH_2), 1.18 (s, 2H, CH_2), 1.61 (m, 2H, CH_2), 1.93 (m, 4H, 2 × CH_2), 2.17 (m, 2H, CH_2), 2.31 (m, 2H, CH_2), 2.42 (m, 4H, 2 × CH_2), 3.29 (m, 2H, CH_2), 4.13 (m, 4H, 2 × CH_2), 5.29 (s, 4H, 2 × An−CH_2), 6.45 (d, 1H, diazole−H_1), 6.72 (d, 4H, 2 × An−$H_{2,7}$), 6.80 (m, 3H, 3 × Ar−H_2), 7.15 (d, 4H, 2 × An−$H_{1,8}$), 7.23 (m, 3H, 3 × Ar−H_3), 7.39 (d, 3H, 3 × Ar−H_1), 7.48 (d, 4H, 2 × An−$H_{3,6}$), 7.60 (m, 3H, 3 × Ar−H_4), 7.74 (d, 4H, 2 × An−$H_{4,5}$), 7.92 (d, 2H, 2 × An−H_{10}), 8.06 (d, 1H, diazole−H_2). ^{13}C NMR (100 MHz, $CDCl_3$, 25 °C, TMS, δ): 156.98, 132.31, 130.87, 129.69, 128.34, 126.67, 125.58, 120.50, 111.21, 67.61, 55.04, 54.63, 49.55, 47.55, 29.67. FAB-MS (*m*/*z*): 1103 (100%) [**2**]$^+$. Anal. Calcd for $C_{69}H_{66}N_8O_6$: C, 75.11; H, 6.03; N, 10.16. Found: C, 74.98; H, 6.18; N, 10.08.

Compound 1. This was subsequently eluted out with chloroform/methanol (96:4 (v/v)) as the eluent. The dark-red solid obtained was recrystallized from acetone. Yield: 35%. Mp: 236 °C. ^{1}H NMR (400 MHz, $CDCl_3$, 25 °C, TMS, δ): 0.81 (m, 2H, CH_2), 1.18 (s, 6H, 3 × CH_2), 2.25 (br s, 1H, NH), 2.44 (d, 2H, CH_2),

(11) (a) Banthia, S.; Samanta, A. *J. Phys. Chem. B* **2006**, *110*, 6437. (b) van Dongen, E. M. W. M.; Dekkers, L. M.; Spijker, K.; Meijer, E. W.; Klomp, L. W. J.; Merkx, M. *J. Am. Chem. Soc.* **2006**, *128*, 10754.
(12) (a) Stryer, L.; Haugland, R. P. *Proc. Natl. Acad. Sci. U.S.A.* **1967**, *58*, 719. (b) Wu, P.; Brand, L. *Anal. Biochem.* **1994**, *218*, 1.
(13) Ramanoudjame, G.; Du, M.; Mankiewicz, K. A.; Jayaraman, V. *Proc. Natl. Acad. Sci. U.S.A.* **2006**, *103*, 10473.
(14) (a) Thiery, C. *Mol. Photochem.* **1970**, *2*, 1. (b) Schäfer, F. P.; Bor, Zs.; Lüttke, W.; Liphardt, B. *Chem. Phys. Lett.* **1978**, *56*, 455. (c) Kopainsky, B.; Kaiser, W.; Schäfer, F. P. *Chem. Phys. Lett.* **1978**, *56*, 458. (d) Ketskemety, I.; Farkas, E.; Toth, Zs.; Gati, L. *Acta Phys. Chem.* **1982**, *28*, 3. (e) Bourson, J.; Mugnier, J.; Valeur, B. *Chem. Phys. Lett.* **1982**, *92*, 430.
(15) Ragunathan, K. G.; Bharadwaj, P. K. *Tetrahedron Lett.* **1992**, *33*, 7581.
(16) Bullpit, M.; Kitching, W.; Doddrell, D.; Adcock, W. *J. Org. Chem.* **1976**, *41*, 760.

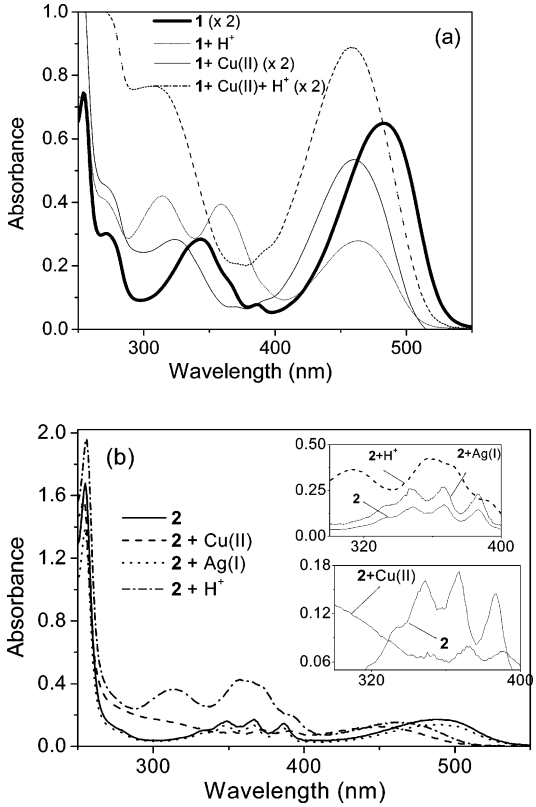

Figure 1. (a) UV−vis spectra of **1**, **1** + Cu(II), **1** + H^+, and **1** + Cu(II) + H^+ (concentration of **1** = 1.6×10^{-5} M) in MeCN. (b) UV-vis spectra of **2**, **2** + Cu(II), **2** + Ag(I), and **2** + H^+ (concentration of **2** = 1.0×10^{-5} M) in MeCN. Inset (above): UV-vis spectra of **2** (solid line), **2** + Ag(I) (dotted line), and **2** + H^+ (dashed line). Inset (bottom): UV−vis spectra of **2**; and **2** + Cu(II) (dotted line).

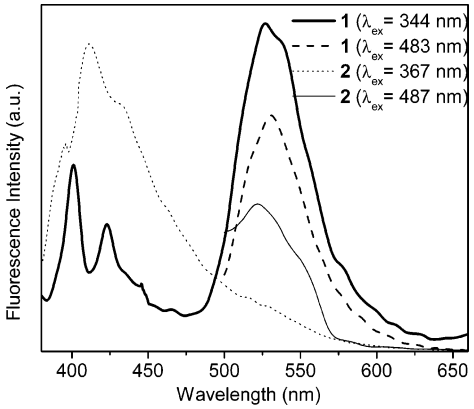

Figure 2. Emission spectra of **1** and **2** (concentration of **1** = 1.0×10^{-6} M and concentration of **2** = 2.5×10^{-6} M) (λ_{ex} are shown in parentheses) in MeCN.

2.65 (t, 2H, CH_2), 2.75 (m, 2H, CH_2), 2.88 (m, 2H, CH_2), 3.13 (m, 2H, CH_2), 3.24 (m, 4H, 2 × CH_2), 3.60 (d, 2H, CH_2), 3.95 (m, 2H, CH_2), 4.13 (m, 2H, CH_2), 4.26 (m, 2H, CH_2), 5.23 (s, 2H, An−CH_2), 6.05 (d, 1H, diazole−H_1), 6.73 (d, 2H, An−$H_{2,7}$), 6.83 (m, 3H, 3 × Ar−H_2), 6.89 (d, 2H, An−$H_{1,8}$), 6.95 (m, 3H, 3 × Ar−H_3), 7.11 (d, 3H, 3 × Ar−H_1), 7.15 (d, 2H, An−$H_{3,6}$), 7.18 (m, 3H, 3 × Ar−H_4), 7.25 (d, 2H, An−$H_{4,5}$), 7.26 (d, 1H, An−H_{10}), 8.26 (d, 1H, diazole−H_2). ^{13}C NMR (100 MHz, $CDCl_3$, 25 °C, TMS, δ): 156.78, 144.70, 135.28, 132.62, 130.14, 122.77, 121.31, 111.99, 102.27, 67.54, 66.36, 55.54, 54.43, 53.48, 52.94, 47.25, 45.71, 29.63. FAB-MS (*m*/*z*): 913 (25%) [**1**]$^+$. Anal. Calcd for $C_{54}H_{56}N_8O_6$: C, 71.03; H, 6.18; N, 12.27. Found: C, 71.20; H, 6.09; N, 12.18.

Synthesis of Protonated Complexes of 1 and 2. To a stirring solution of either ligand (0.1 mmol) in acetonitrile was added a dilute perchloric acid solution, and the solution was stirred for 2 h at room temperature and then filtered. The filtrate upon evaporation at room temperature for 3−4 days afforded a deep-yellow crystalline solid that was collected by filtration, washed with ether, and dried under a vacuum for solid-state emission measurements. For [**1**·H]$^+$ complex. Yield: 75%; ESI-MS (*m*/*z*): 914 (20%) [**1**·H]$^+$. Anal. Calcd for $C_{54}H_{57}ClN_8O_{10}$: C, 63.99; H, 5.67; N, 11.06. Found: C, 64.20; H, 5.81; N, 10.89. For the [**2**·H]$^+$ complex. Yield: 60%. ESI-MS (*m*/*z*): 1104 (100%) [**2**·H]$^+$ and 1204 (35%) [(**2**·2H)-ClO_4]$^+$. Anal. Calcd for $C_{69}H_{68}Cl_2N_8O_{14}$: C, 63.54; H, 5.25; N, 8.59. Found: C, 63.34; H, 5.29; N, 8.68.

Synthesis of the Cd(II) Complex of 1. To a stirring solution of ligand **1** (0.1 mmol) in dry acetonitrile was added an acetonitrile solution of $Cd(NO_3)_2 \cdot 4H_2O$ (0.1 mmol) followed by NaCl (0.1 mmol), and the solution was stirred for 2 h at room temperature. After filtration, the filtrate left at room temperature overnight afforded an orange crystalline solid as the desired product. The solid was collected by filtration, washed several times with cold acetonitrile, and dried under a vacuum for use in emission measurements. Yield: 65%. ESI-MS (*m*/*z*): 1104 (25%) [Cd(**1**)-$NO_3 \cdot H_2O$]$^+$. Anal. Calcd for $C_{54}H_{58}N_{10}O_{13}Cd$: C, 55.55; H, 5.01; N, 12.00. Found: C, 55.43; H, 5.09; N, 12.08.

Synthesis of the Cu(II) Complex of 2. To a stirring solution of **2** (0.1 mmol) in dry ethanol (20 mL) was added an ethanolic solution (5 mL) of $Cu(ClO_4)_2 \cdot 6H_2O$ (0.1 mmol) followed by NaCl (0.1 mmol), and the solution was stirred for 2 h at room temperature. After filtration, the filtrate was allowed to evaporate at room temperature, whereupon a greenish-yellow crystalline solid separated. The solid was collected by filtration, washed with diethyl ether, and dried under a vacuum for use in emission measurements. Yield: 72%. ESI-MS (*m*/*z*): 1268 (45%) [Cu(**2**)ClO_4]$^+$. Anal. Calcd for $C_{69}H_{66}N_8O_{10}ClCu$: C, 65.45; H, 5.25; N, 8.85. Found: C, 65.36; H, 5.30; N, 8.81.

Physical Measurements. Compounds **1** and **2** were characterized by elemental analyses, ^{1}H NMR, ^{13}C NMR, and mass (positive ion) spectroscopy. ^{1}H NMR and ^{13}C NMR spectra were recorded on a JEOL JNM-LA400 FT (400 and 100 MHz, respectively) instrument in $CDCl_3$. FAB mass (positive ion) data were obtained from a JEOL SX 102 /DA-6000 mass spectrometer using argon as the FAB gas at 6 kV and 10 mA, with an accelerating voltage of 10 kV, and the spectra were recorded at 298 K. ESI mass spectra were recorded on a Micromass Quattro II triple−quadrupole mass spectrometer. The ESI capillary was set at 3.5 kV, and the cone voltage was 40 V. Melting points were determined with an electrical melting point apparatus by PERFIT, India, and were uncorrected. UV−vis spectra were recorded on a Jasco V-570 spectrophotometer at 293 K, and the average of three measurements was taken. The deviations in molar absorption coefficients were in the last digit only. Steady-state fluorescence spectra were obtained using a PerkinElmer LS 50B luminescence spectrometer at 293 K with an excitation and emission band pass of 5 nm. Steady-state fluorescence anisotropy data were obtained using a PerkinElmer LS 55 fluorimeter at 293 K with a slit width of 5 nm and an integration time of 40 s.

Fluorescence quantum yields of all of the compounds were determined by comparing the corrected spectrum with that of anthracene ($\phi = 0.297$) in ethanol,[17] taking the area under the total

(17) Birks, J. B. *Photophysics of Aromatic Molecules*; Wiley-Interscience: New York, 1970.

Table 1. Fluorescence Output of **1** and **2** with Different Ionic Inputs[a]

	Quantum yield ϕ (enhancement factor)		
	$\phi_{diazole}$ (λ_{ex} = 344 nm)	$\phi_{anthracene}$ (λ_{ex} = 344 nm)	$\phi_{diazole}$ (λ_{ex} = 483 nm)
1	0.0008	0.0003	0.0008
1 + Mn(II)	0.0015 (2)	0.0004 (1)	0.0017 (2)
1 + Fe(II)	0.0662 (83)	0.0006 (2)	0.0674 (84)
1 + Co(II)	0.0008 (1)	0.0003 (1)	0.0007 (<1)
1 + Ni(II)	0.0005 (<1)	0.0003 (1)	0.0004 (<1)
1 + Cu(II)	0.1434 (179)	0.0015 (5)	0.1460 (183)
1 + Zn(II)	0.1206 (151)	0.0008 (3)	0.1199 (150)
1 + Cd(II)	0.2549 (319)	0.0006 (2)	0.2446 (306)
1 + Ag(I)	0.0372 (47)	0.0004 (1)	0.0363 (45)
1 + Tl(I)	0.0011 (1)	0.0003 (1)	0.0010 (1)
1 + H^+	0.2209 (276)	0.0005 (2)	0.2181 (273)
1 + Cu(II) + H^+	0.1947 (243)	0.0014 (5)	0.2001 (250)
2	0.0006	0.0046	0.0006
2 + Mn(II)	0.0034 (6)	0.0023 (<1)	0.0037 (6)
2 + Fe(II)	0.0264 (44)	0.0033 (<1)	0.0278 (46)
2 + Co(II)	0.0015 (3)	0.0021 (<1)	0.0016 (3)
2 + Ni(II)	0.0013 (2)	0.0020 (<1)	0.0013 (2)
2 + Cu(II)	0.1599 (267)	0.0696 (15)	0.1640 (273)
2 + Zn(II)	0.0286 (48)	0.0042 (<1)	0.0302 (50)
2 + Cd(II)	0.0022 (4)	0.0027 (<1)	0.0024 (4)
2 + Ag(I)	0.1136 (189)	0.0034 (<1)	0.1154 (192)
2 + Tl(I)	0.0012 (2)	0.0024 (<1)	0.0012 (2)
2 + H^+	0.1644 (274)	0.0562 (12)	0.1688 (281)

[a] Experimental conditions: medium, dry MeCN; concentration of **1**, 1.6×10^{-5} M; concentration of ionic input, 10^{-4} M; concentration of **2**, 10^{-5} M; concentration of ionic input, 10^{-4} M. Excitation at 344 and 483 nm for **1** and 367 and 487 nm for **2**, with an excitation band pass of 5 nm; emission band pass, 5 nm; temperature, 298 K; $\phi_{anthracene}$ and $\phi_{diazole}$ were calculated by the comparison of the corrected spectrum with that of anthracene and quinine sulfate respectivley, taking the area under the total emission. The error in ϕ is within 10% in each case, except in the case of free ligands, where the error in ϕ is within 15%.

emission. On the other hand, emission quantum yields due to the diazole fluorophore in **1** and **2** were checked by comparing the corrected spectrum with that of quinine sulfate[17] in 1 N H_2SO_4. The fluorescence measurements in the solutions were carried out at $\sim 10^{-6}$ M concentration, unless otherwise specified. The solid-state emission spectra were recorded using a Fluorolog3, model FL3-22, SPEX spectrometer excited at ~350 nm with a 450 W xenon lamp at a band pass of 2 nm, and the integration time was kept at 0.2 s. The complex stability constants K_s were determined[18] from the change in absorbance or fluorescence intensity resulting from the titration of dilute solutions ($\sim 10^{-5}-10^{-6}$ M) of the fluorophoric systems against the metal ion concentration. The reported values gave good correlation coefficients (≥ 0.99).

Results and Discussion

UV−Vis Absorption Spectroscopy. In dry MeCN, cryptand $\mathbf{L_0}$ shows only negligible absorption in the region of interest. The parent chromophore 4-*N*,*N*-dimethyl-7-nitrobenzofurazan gives an absorption[19] at 478 nm in MeCN because of intramolecular charge transfer (ICT) from the donor nitrogen to the acceptor NO_2 group, and the single diazole-substituted cryptand ($\mathbf{L_1}$ in Scheme 1) shows[9b] this ICT band at the same position. Similarly, 9-methylanthracene exhibits[17] the (0,0) band at 388 nm and vibrational structures at 368, 350, and 333 nm, and they do not show[20] any perceptible shift in mono- and bis-anthryl-substituted $\mathbf{L_0}$. The diazole ICT band position in **1** and **2** does not shift much,[21] although anthryl band positions and their nature[17] show significant changes presumably due to movement[9c] of the side arms, causing interactions between the two moieties. These changes are more prominent in the case of **1**. Thus, in **1** the anthryl bands appear as a broad band centering at 344 nm with shoulders at 365 and 387 nm. In **2**, on the other hand, the (0,0) band appears at 387 nm along with vibrational structures at 367 and 350 nm. The intensities of the anthryl bands in **2** are more than double those in **1** in any solvent as a result of different magnitudes of movement of the side arms in the two cases. In addition, both **1** and **2** exhibit two more bands at 271 and 254 nm because of the $\pi-\pi$ interaction of the phenyl group of the cryptand side arm with anthracene in the ground state and in the anthracene $S_0 \rightarrow S_3$ transition, respectively. The ICT band in **1** is solvatochromic in nature; it absorbs at 462 nm in nonpolar cyclohexane and at 496 nm in relatively polar DMSO. This solvatochromic behavior is similar to that of 4-*N*,*N*-dimethyl-7-nitrobenzofurazan as reported.[19]

The ICT band in **1** blue-shifts by 2−9 nm (Table ST2)[21] in the presence of a metal ion (except Cu(II)), without moving the positions of the other bands. In the presence of Cu(II), both the ICT band and the 344 nm band of the anthryl moiety blue-shift by ~28 nm, indicating a different mode of binding for this metal ion in contrast to others probed. Upon protonation, the ICT band blue-shifts, and because of the decrease in donor−acceptor interaction, the molar absorptivity decreases. However, protonation also results in blue shifts of all of the anthryl bands with higher molar absorptivity (Table ST2 and part a of Figure 1) from enhanced charge-transfer character[9c] as a result of orientational modification of the anthracene chromophores.

(18) (a) Fery-Forgues, S.; Le Bries, M.-T.; Guetté, J.-P.; Valeur, B. *J. Phys. Chem.* **1988**, *92*, 6233. (b) Bag, B.; Bharadwaj, P. K. *J. Phys. Chem. B* **2005**, *109*, 4377.
(19) Saha, S.; Samanta, A. *J. Phys. Chem. A* **1998**, *102*, 7903.
(20) Bag, B.; Bharadwaj, P. K. *J. Lumin.* **2004**, *110*, 85.
(21) See the Supporting Information section.

Similar solvatochromic behavior is observed for the ICT band in **2**. This band blue-shifts in the presence of a metal ion (except Cu(II)) by 3−10 nm (Table ST4),[21] without affecting the anthryl bands. In the presence of Cu(II), the ICT band blue-shifts by 37 nm, whereas the anthryl bands red-shift by very small amounts (part b of Figure 1). In the presence of protons, **2** gives results similar to those in the case of **1**.

Stokes' shift analysis as a function of solvent polarity[22,23] results in the estimation of the difference in dipole moments between the excited state and the ground state and quantifies the extent of the charge-transfer process in the excited state. The contribution of the solvent-induced dipole moment and the polarizability of the solute are taken into consideration for determining the excited-state dipole moment of the ligands, using a modified Lippert−Mataga equation.[24] On the basis of the plot and its linear regression derived thereof, the excited-state dipole moments (μ_e) for **1** and **2** are estimated to be 19 and 16 D, respectively. Geometrical optimizations for the systems are carried out by the semiempirical AM1 method (gradient <0.001, Hyperchem version 7.0, Hypercube Inc.). Attachment of electron-withdrawing and electron-donating group(s) increases the ground-state dipole moment,[21] which favors charge separation. This dipole moment value is further increased in the excited state, which suggests complete charge separation in the excited state.

Emission of Metal-Free Ligands. Compound **1** shows dual emissions, the exact nature of which depends on the wavelength of light used for excitation. In MeCN, upon excitation at 344 nm, where the band due to anthracene in **1** absorbs predominantly, emissions due to both anthracene and diazole appear with low intensity (Figure 2) as a result of PET being operational. However, the appearance of both of the bands suggests a small amount of resonance energy transfer from the anthracene to the diazole moiety. When excited at 483 nm, an emission due to the diazole moiety alone is observed. The fluorescence quantum yields $\phi_{anthracene}$ and $\phi_{diazole}$ were determined at the excitation wavelengths of 344 and 483 nm, respectively. The low quantum yield values observed (Table 1) are due to efficient PET from the receptor nitrogen to the fluorophores. Compound **2** exhibits a similar behavior except that, in this case, a well-resolved emission typical of 9-alkyl-substituted[17] anthracene can be observed (Figure 2). The (0,0) band of the locally excited anthracene emission is centered at ∼400 nm in all of the solvents studied. The emission due to the diazole moiety is found to be solvatochromic in nature,[21] and the emissions from the two fluorophores do not overlap.

Emission in the Presence of Metal Ions or Protons and Complex Stability Constants. When a transition-metal ion is added to **1** in MeCN, the metal occupies[25] the tren-end of the cavity, engaging the nitrogen lone pairs that block PET. However, when **1** is excited at 344 nm, no substantial enhancement of anthracene monomer emission is observed, unlike in previous cases.[9a,c] The enhancement factor remains within a limit of ∼5 (Table 1), which is quite ineffective. Instead, a large emission at ∼520 nm assignable[9b] to the diazole moiety is observed (parts a and b Figure 3) as a result of a significant amount of fluorescence resonance energy transfer from the excited anthracene to the diazole, where the metal ion acts as a conduit. Among the 3D transition-metal ions, Cu(II) and Zn(II) show large enhancement of fluorescence with respect to metal-free **1**, whereas Fe(II) exhibits one order of magnitude less enhancement. The highest enhancement of diazole emission is observed with Cd(II). Also, Ag(I) gives noticeable enhancement. The data are collected in Table 1.

Compound **2** behaves quite similarly, although unlike **1**, only Cu(II) and Ag(I) exhibit significant increases in emission. Other metal ions used as inputs show less enhancement (Table 1).

Thus, the signal transduction mechanism operational here makes the present systems unique compared to other signaling systems. The response of **1** and **2** can be compared with that of simple PET-based fluorophore−spacer−receptor systems, which comprise either diazole or anthracene.[9,20] Here, **1** and **2** act as turn-on sensors in the presence of specific metal ions. Because Cd(II) shows the highest quantum yield among the metal ions studied with both systems, it is titrated with **1**, and the emission band due to the diazole moiety at ∼520 nm is monitored. The intensity of the emission gradually increases and attains a maximum[21] when 1 equiv of the metal ion is added. Thereafter, no change in the intensity is observed (Figure 4), indicating a 1:1 formation. When **2** is titrated with Cu(II) and Ag(I), similar behavior is observed (Figure 4).

Hydrated metal perchlorate and nitrate salts can generate protons in organic solvents. To verify that the fluorescence enhancement is due to the metal ion only and not to protonation, certain controlled experiments[9a,26] were carried out. Moreover, different metal ions give different extents of enhancement. If the proton generation in the medium by the metal salts is responsible, then the extent of enhancement should have been almost the same for all of the metal salts used. In MeCN, emission as a result of the diazole moiety enhances by a large factor (∼275 times for **1** and **2**) in the presence of $HClO_4$ (1×10^{-3} M) (parts a and c of Figure 3). Substantial fluorescence enhancement is observed, suggesting that both of the nitrogen atoms, attached to the fluorophores, are protonated. The diazole emission in the **1**⊂Cu(II) complex is further increased when it is treated with a $\sim 10^{-3}$ M $HClO_4$ solution. The same types of changes are observed when **1**⊂Co(II) and **1**⊂Zn(II) complexes are protonated with a $\sim 10^{-3}$ M $HClO_4$ solution.

We carried out proton titration with **1** and **2** as well as **1**⊂Cu(II) to observe the extent of the changes in the fluorescence enhancement. Maximum enhancements for **1**

(22) Lippert, E. Z. *Naturforsch*. **1955**, *10A*, 541.
(23) Mataga, N.; Kaifu, Y.; Koizumi, M. *Bull. Chem. Soc. Jpn*. **1956**, *29*, 465.
(24) Herbich, J.; Kapturkiewicz, A. *J. Am. Chem. Soc*. **1998**, *120*, 1014.
(25) (a) Chand, D. K.; Bharadwaj, P. K. *Inorg. Chem*. **1996**, *35*, 3380. (b) Ghosh, P.; Gupta, S. S.; Bharadwaj, P. K. *J. Chem. Soc., Dalton Trans*. **1997**, 935.
(26) Ramachandram, B.; Saroja, G.; Sankaran, N. B.; Samanta, A. *J. Phys. Chem. B* **2000**, *104*, 11824.

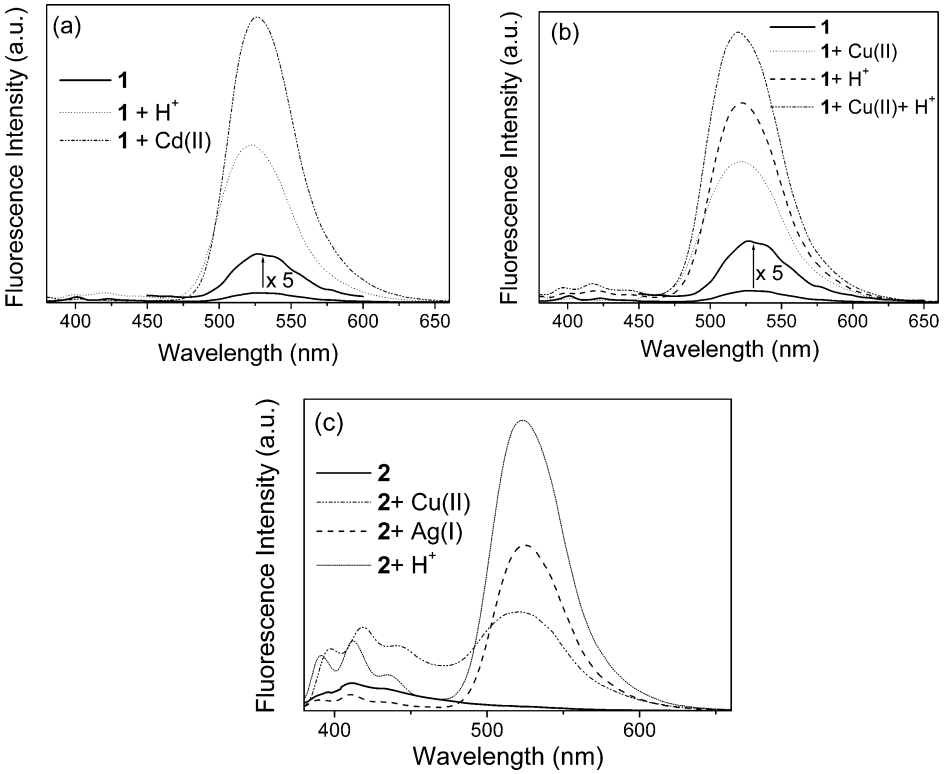

Figure 3. (a) Emission spectra of **1**, **1** + Cd(II), and **1** + H^+ (concentration of 1 = 1.0×10^{-6} M) in MeCN. (b) Emission spectra of **1**, **1** + Cu(II), and **1** + H^+, **1** + Cu(II) + H^+ (concentration of **1** = 2.5×10^{-6} M) in MeCN. (c) Emission spectrum of **2**, **2** + Cu(II), **2** + Ag(I), and **2** + H^+ complexes (concentration of **2** = 1.0×10^{-6} M) in MeCN.

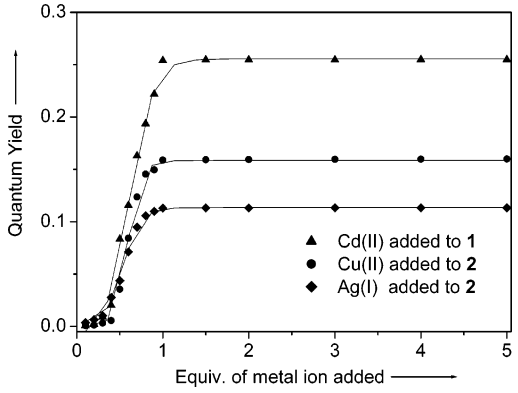

Figure 4. Plot of the quantum yields ($\phi_{diazole}$) of **1** and **2** (concentration of **1** and **2** = 1.4×10^{-6} M) as a function of equivalents of Cd(II) ions for **1** (λ_{ex} = 344 nm) and Cu(II) and Ag(I) ions for **2** (λ_{ex} = 367 nm) in MeCN.

and **2** are observed after the addition of 2 equivs of protons, whereas the enhancement is saturated after the addition of 1 equiv of protons to **1**⊂Cu(II) (Figure 5).

In most of the cases, K_s cannot be determined with proper accuracy because the changes in fluorescence/absorbance intensities are not substantial. For **1** and Cd(II), the K_s value of 1.06×10^6 M^{-1} can be determined. The K_s values determined from the fluorescence intensity data for **2** with Cu(II) and Ag(I) are found to be 1.42×10^6 and 8.61×10^5 M^{-1}, respectively. Although the data on complex stability constants are not complete, it is found that, in cases where substantial fluorescence increases are observed upon the addition of a metal salt or protons, the complex stability constants are on the order of 10^6 M^{-1}, which is quite similar to those of other systems reported in the literature.[18b,27]

Solid-State Fluorescence and Interchromophoric Distance Calculation in Solution. To confirm the absence[10b] of fluorescence resonance energy transfer in the solid state, solid-state fluorescence measurements for **1**⊂Cd(II), **1**·H^+, **2**⊂Cu(II), and **2**·H^+ were undertaken, each of which showed only anthracene monomer emission when excited at the corresponding anthryl absorption maximum (Figure 6). When these complexes are dissolved in MeCN, quantum yields for the fluorophores similar to those in the corresponding solution studies are obtained.

The interchromophoric distances can be estimated by steady-state energy-transfer experiments following a protocol (eq 1) reported in the literature.[28] The interchromophoric

$$E = \frac{R_0^6}{R_0^6 + R^6} \tag{1}$$

distances (R) due to dipole−dipole interaction depend upon the orientational factor (κ ; eq 2).

$$R_0 = 9.78 \times 10^3(\eta^{-4}\phi_d\kappa^2 J)^{1/6}\ \text{Å} \tag{2}$$

(27) (a) Rurack, K.; Bricks, J. L.; Schulz, B.; Maus, M.; Reck, G.; Resch-Genger, U. *J. Phys. Chem. A* **2000**, *104*, 6171. (b) Kollmannsberger, M.; Rurack, K.; Genger-Resch, U.; Daub, J. *J. Phys. Chem. A* **1998**, *102*, 10211.
(28) Mugnier, J.; Pouget, J.; Bourson, J.; Valeur, B. *J. Lumin.* **1985**, *33*, 273.

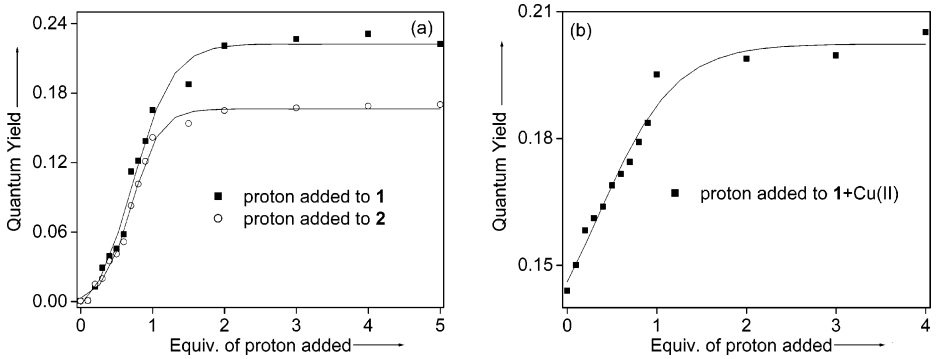

Figure 5. Plot of the quantum yields ($\phi_{diazole}$) of **1** and **2** (concentration of **1** and **2** = 1.4×10^{-6} M) as a function of equivalents of H^+ ions for (a) **1** (λ_{ex} = 344 nm) and **2** (λ_{ex} = 367 nm) and for (b) the **1** + Cu(II) complex (λ_{ex} = 344 nm) in MeCN.

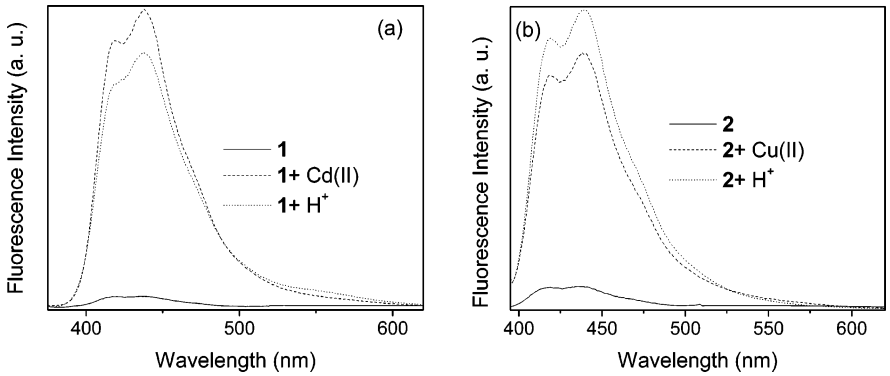

Figure 6. (a) Solid-state emission spectra of **1**, **1** + Cd(II), and **1** + H^+ complexes (λ_{ex} = 344 nm). (b) Solid-state emission spectra of **2**, **2** + Cu(II), and **2** + H^+ complexes (λ_{ex} = 367 nm).

Table 2. Interchromophoric Distances of **1** and **2** with Different Ionic Inputs

	E (%)	ϕ_d[a]	J (M^{-1} cm^3)	$\langle\kappa^2\rangle_{max}$[b]	$\langle\kappa^2\rangle_{min}$[b]	$R_{0,avg}$[c]	R_{avg}[c,d]
1	2	0.0004	6.32×10^{-15}	1.17	0.49	9	17
1 + Cd(II)	74	0.0401	7.38×10^{-15}	1.14	0.49	21	18
2	4	0.0003	6.37×10^{-15}	1.23	0.46	9	15
2 + Cu(II)	69	0.0422	7.49×10^{-15}	1.78	0.31	20	18
2 + Ag(I)	79	0.0458	7.34×10^{-15}	1.03	0.52	20	16

[a] Quantum yield of the anthracene-substituted cryptand in the absence of a diazole acceptor in MeCN. [b] Limits on κ^2 are obtained by the measurements of the fluorescence anisotropy of the donor and acceptor fluorophores. [c] All of the distances are in angstroms. [d] Uncertainty in the derived intramolecular separation of approximately ±15% about the limit of R.

The limits on κ^2 are obtained[29] by measurements of the fluorescence anisotropy of the donor and acceptor of the fluorophores. Therefore, these measurements can minimize uncertainties in the calculated interchromophoric distances in the solution state. The interchromophoric distances, in the cases of metal complexes of **1** and **2**, afford values in the range of ~18 Å that are larger than the distances observed in the cases of free **1** and **2** (Table 2). The changes in the interchromophoric distances in the metal complexes tune them to be specific in the involved fluorescence resonance energy transfer processes.

Conclusion

In conclusion, an aza cryptand is shown to be an ideal skeleton for the addition of different fluorophores that show significant fluorescence resonance energy transfer in the presence of transition-metal ions. Here, two cryptand-based fluorescence signaling systems are mentioned, which exhibit very low monomeric fluorescence and resonance energy transfer in the absence of a metal ion or proton. However, in **1**, the fluorescence resonance energy transfer is found to be quite significant in the presence of Cd(II), whereas in **2**, a similar behavior is observed in the presence of Cu(II) and Ag(I). Both systems also exhibit energy-transfer processes in the presence of protons. The metal ion or proton not only blocks the PET by engaging the nitrogen lone pairs but also induces a structural modification of the receptor core so that appreciable energy transfer can be observed. Thus, these systems not only exhibit fluorescence in the presence of transition-metal ions but also induce fluorescence resonance energy transfer from anthracene to the diazole moiety. Thus, these processes provide a design for the next generation of fluorescence signaling systems and a route to effect photo-

(29) Dale, R. E.; Eisinger, J.; Blumberg, W. E. *Biophys. J.* **1979**, *26*, 161.

induced charge separation. We are presently engaged in these aspects along with the rate of fluorescence resonance energy transfer by time-resolved fluorescence spectroscopy.

Acknowledgment. Financial support for this work is from the Department of Science and Technology, New Delhi, India, and is gratefully acknowledged. K.K.S. thanks CSIR, New Delhi, India, for a Senior Research Fellowship. We thank Dr. Anindya Datta from the Indian Institute of Technology, Bombay, for fluorescence anisotropy data.

Supporting Information Available: Characterization of the ligands **1** and **2**: FAB-MS, ^{13}C NMR, ^{1}H NMR, UV−vis, and fluorescence spectral data. This material is available free of charge via the Internet at http://pubs.acs.org.

IC700506R